CONDENSED MATTER PHYSICS

Graphene-mediated ferromagnetic coupling in the nickel nano-islands/graphene hybrid

Min Gao[1,2†], Xiaowen Han[1,2†], Wenjing Liu[1], Ziao Tian[1], Yongfeng Mei[3], Miao Zhang[1], Paul K. Chu[4], Erjun Kan[5], Tao Hu[6], Yongping Du[5]*, Shan Qiao[1,2]*, Zengfeng Di[1,2]*

Nanoscale magnetic structures are fundamental to the design and fabrication of spintronic devices and have exhibited tremendous potential superior to the conventional semiconductor devices. However, most of the magnetic moments in nanostructures are unstable due to size effect, and the possible solution based on exchange coupling between nanomagnetism is still not clear. Here, graphene-mediated exchange coupling between nanomagnets is demonstrated by depositing discrete superparamagnetic Ni nano-islands on single-crystal graphene. The heterostructure exhibits ideal two-dimensional (2D) ferromagnetism with clear hysteresis loops and Curie temperature up to 80 K. The intrinsic ferromagnetism in graphene and antiferromagnetic exchange coupling between graphene and Ni nano-islands are revealed by x-ray magnetic circular dichroism and density functional theory calculations. The artificial 2D ferromagnets constitute a platform to study the coupling mechanism between complex correlated electronic systems and magnetism on the nanoscale, and the results and concept provide insights into the realization of spin manipulation in quantum computing.

INTRODUCTION

Spintronic devices with high processing speed and small power consumption have large potential and superiority over conventional semiconductor devices in data storage and information processing by using the spin degree of freedom (*1*–*4*). The continuous pursuit to reduce the size of spintronic devices, increase the density integration, and decrease the cost of data storage has spurred the development of nanoscale magnetic structures (*5*–*10*). In particular, magnetic nano-islands provide a useful tool to investigate the spin interactions on the nanoscale and monitor the evolution and impact of magnetization (*11*, *12*). However, it is still challenging to stabilize the nanoscale magnetic moments in applications such as quantum-based computation and spintronics. According to the theoretical prediction, a weakly reactive substrate such as graphene (*13*–*16*) can mediate the exchange coupling between nanomagnetic structures. The proximity-induced anomalous Hall effect (AHE) has been observed from graphene in a magnetic Fe_3O_4 nanoparticle array (*17*). In this system, spin-orbit coupling is considered to be enhanced in graphene due to the proximity effect leading to mediation of the interaction between the nano-scale Fe_3O_4 magnets. However, there is no direct evidence on the change of magnetic moments in graphene; therefore, the detailed exchange interaction between graphene and nanomagnets is still unclear.

In this work, a graphene-mediated exchange coupling ferromagnetic system is fabricated by depositing discrete Ni nano-islands on single-crystal graphene as schematically illustrated in Fig. 1A. The Ni nano-islands behave as superparamagnetism due to the nanoscale size (*18*). The temperature-dependent magnetic measurement shows the ideal global two-dimensional (2D) ferromagnetism as manifested by clear hysteresis loops and a Curie temperature of 80 K, which is much higher than the block temperature of freestanding superparamagnetic Ni nano-islands. The ferromagnetism in the Ni nano-islands/graphene system is ascribed to antiferromagnetic exchange coupling between the superparamagnetic Ni nano-islands and ferromagnetic graphene as confirmed by x-ray magnetic circular dichroism (XMCD) measurements and density functional theory (DFT) calculations.

RESULTS AND DISCUSSION

The observation of ferromagnetism in the Ni nano-islands/graphene system

The single-crystal monolayer graphene is grown on intrinsic Ge (110) by chemical vapor deposition and transferred to a 300-nm SiO_2/Si substrate by the polymethyl methacrylate (PMMA)–assisted wet transfer method (*19*). Raman scattering and Raman mapping (fig. S1) show that the ratio of I_{2D}/I_G is about 1.7 and the intensity of I_D approaches 0, indicating that the transferred graphene consists of a monolayer and has high crystalline quality (*20*). The high-quality monolayer graphene is believed to exhibit the exceptional feature of 2D electron gas (2DEG) (*21*). An 8-nm-thick Ni is deposited on the graphene/SiO_2/Si substrate by electron beam evaporation (see Materials and Methods and fig. S2). Owing to the poor wettability and small surface free energy of graphene (*22*), the Ni layer is dispersed randomly to form discrete nano-islands on graphene, as revealed by atomic force microscopy (AFM) (Fig. 1, B and C). The cross-sectional scanning transmission electron microscopy (STEM) image and corresponding energy dispersive spectroscopy (STEM-EDS) data in Fig. 1D disclose that the Ni nano-islands are disconnected.

[1]State Key Laboratory of Functional Materials for Informatics, Shanghai Institute of Microsystem and Information Technology, Chinese Academy of Sciences, 865 Changning Road, Shanghai 200050, China. [2]Center of Materials Science and Optoelectronics Engineering, University of Chinese Academy of Sciences, Beijing 100049, China. [3]Department of Materials Science, Fudan University, Shanghai 200433, China. [4]Department of Physics, Department of Materials Science and Engineering, and Department of Biomedical Engineering, City University of Hong Kong, Tat Chee Avenue, Kowloon, Hong Kong, China. [5]Department of Applied Physics and Institution of Energy and Microstructure, Nanjing University of Science and Technology, Nanjing 210094, China. [6]Beijing Academy of Quantum Information Sciences, Beijing 100193, China.
*Corresponding author. Email: qiaoshan@mail.sim.ac.cn (S.Q.); njustdyp@njust.edu.cn (Y.D.); zfdi@mail.sim.ac.cn (Z.D.)
†These authors contributed equally to this work.

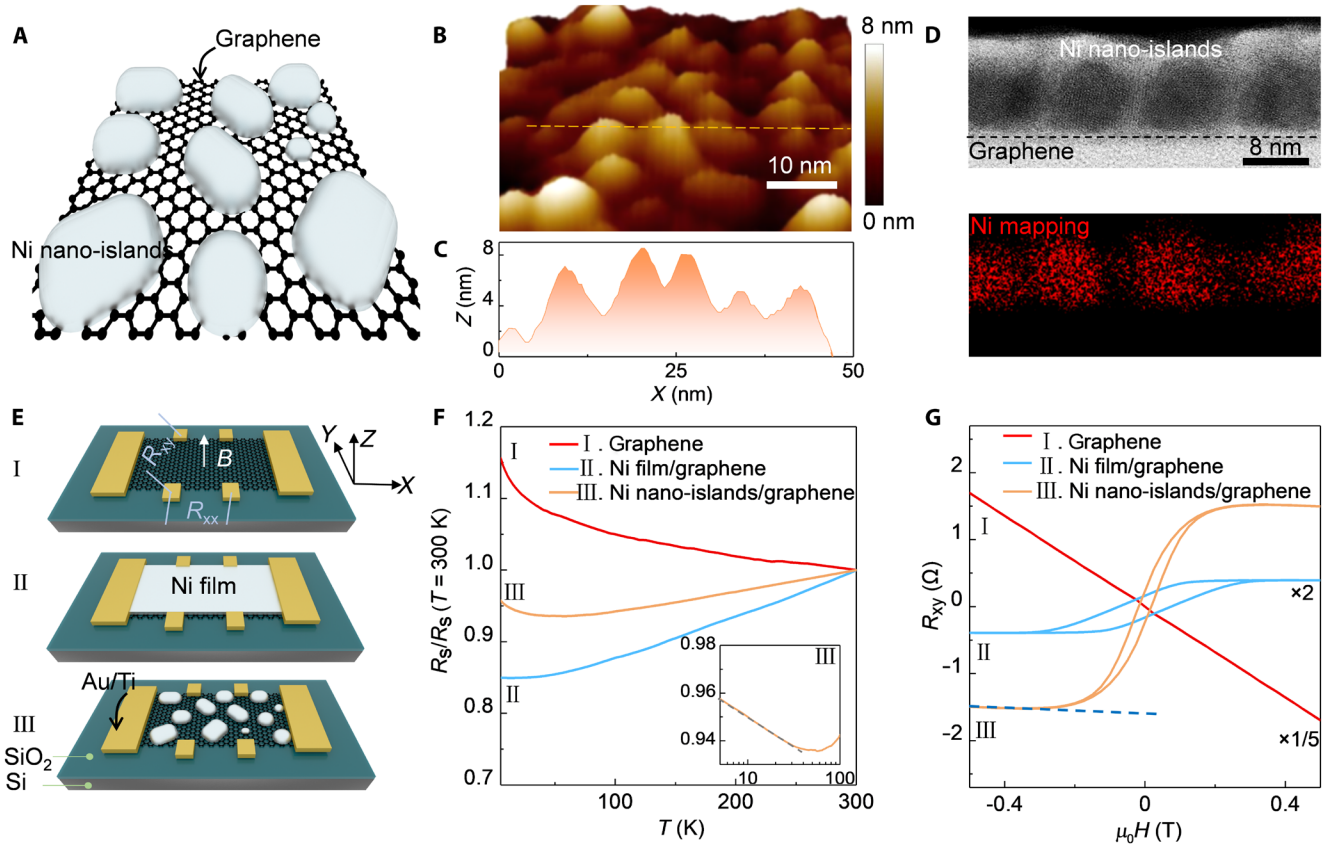

Fig. 1. Characterization of Ni nano-islands/graphene. (**A**) Schematic of the construction of the 2D ferromagnetic system consisting of discrete Ni nano-islands and single-crystal graphene. (**B**) AFM image of Ni nano-islands/graphene. (**C**) Line scan along the dashed line in (B). (**D**) Cross-sectional STEM image and corresponding STEM-EDS map of Ni. (**E**) Schematic of the configurations of the graphene (I), Ni film/graphene (II), and Ni nano-islands/graphene (III). (**F**) Sheet resistance (R_s) of graphene (red line I), Ni film/graphene (blue line II), and Ni nano-islands/graphene (orange line III) versus temperature at a zero field. All of the resistance curves are normalized by the values at $T = 300$ K, and the inset shows the linear dependence of R-ln$T$ for Ni nano-islands/graphene at low temperature. (**G**) Perpendicular magnetic field dependence of the Hall resistance R_{xy} of graphene (red line I), Ni film/graphene (blue line II), and Ni nano-islands/graphene (orange line III) at 5 K. The dashed line indicates the appearance of NHE.

The Ni nano-islands/graphene hybrid is made into a Hall bar device (Materials and Methods and Supplementary Text) to conduct a series of transport measurements. Figure 1F shows the normalized temperature-dependent sheet resistance $R_s(T)$ of the Ni nano-islands/graphene system (orange line III) at zero magnetic field in comparison with graphene (red line I) and Ni film (30 nm)/graphene (blue line II). In pure graphene (red line I in Fig. 1F and fig. S3A), R_s increases as the temperature is reduced from 300 to 5 K and exhibits a ln$T$ dependence due to the weak localization behavior commonly observed from 2D materials at low temperature (*23*–*25*). The Ni film/graphene (blue line II in Fig. 1F and fig. S3B) shows the typical metallic (*26*) behavior together with obvious resistance deduction at high temperature and almost constant resistance at low temperature. However, the sheet resistance of the Ni nano-islands/graphene system (orange line III) behaves quite differently, showing a unique transition. When the temperature deceases from 300 to 50 K, the sheet resistance declines since the total resistance R_s consists of the combination of Ni nano-islands and metallic graphene, and the temperature dependence of R_s is similar to that of metals. However, upon further cooling, the sheet resistance increases gradually and shows a linear relationship with ln$T$ (inset of Fig. 1F and fig. S3C), which can be attributed to the typical weak localization behavior of graphene. In addition, the metal-insulator transition of graphene induced by the additive Ni nano-islands also contributes to the increment of total resistance R_s, as suggested by the DFT calculations afterward. Figure 1G shows the corresponding Hall resistances as a function of perpendicular magnetic fields at 5 K. For pure graphene (red line I), the Hall resistance exhibits a linear trace as expected for the normal Hall effect (NHE). The Hall resistance of the Ni film/graphene (blue line II) shows a hysteresis loop indicating the existence of ferromagnetism and AHE. The Hall resistance in Ni nano-islands/graphene shows a hysteresis loop from ~−0.2 to ~0.2 T, which suggests the presence of ferromagnetism and AHE, while at high magnetic fields, the Hall resistance loop closes and evolves into a slight linear trace indicating the appearance of NHE (indicated by the dashed line in Fig. 1G). Therefore, the total Hall resistance in the Ni nano-islands/graphene system can be expressed as (*27*, *28*)

$$R_{xy} = R_{xy}^{NHE} + R_{xy}^{AHE} = \alpha \mu_0 H + \beta M \quad (1)$$

where $R_{xy}^{NHE} = \alpha \mu_0 H$ represents the NHE component due to the Lorentz force, α is the ordinary Hall coefficient, and $R_{xy}^{AHE} = \beta M$ is the AHE component in which β is the anomalous Hall coefficient

related to the carrier density and M is magnetization. Coexistence of NHE and AHE in the Ni nano-islands/graphene system suggests that graphene is magnetically coupled with the Ni nano-islands, and consequently, global ferromagnetism is formed. The angle-dependent R_{xy}^{AHE} curves in fig. S4 suggest that the c axis is the easy magnetization direction. In addition, both the saturation value of R_{xy}^{AHE} and the coercive field decrease as the rotation angle increases due to the decrease of projection of the applied magnetic field toward the c axis.

The Curie temperature is defined as 80 K in the Ni nano-islands/graphene system

To further explore the ferromagnetic properties of the Ni nano-islands/graphene system, the Hall resistance R_{xy} is measured at different temperatures (fig. S5) and the extracted R_{xy}^{AHE} loops are displayed in Fig. 2A. When the temperature is below 60 K, the AHE curves show clear hysteresis loops, indicating a long-range ferromagnetic order. When the temperature is over 60 K, the loops vanish, indicating that the long-range ferromagnetic order is destroyed by the thermal fluctuation and the system evolves into a paramagnetic phase. Thus, the Curie temperature T_c of the Ni nano-islands/graphene system is found to be ~60 K. To fully elucidate the ferromagnetic characteristics of the Ni nano-islands/graphene system, the magnetic properties are determined on the Magnetic Property Measurement System (MPMS-3, Quantum Design). After subtracting the diamagnetic contribution from the SiO_2/Si substrate (fig. S6), the magnetic hysteresis loops can be deduced as shown in Fig. 2B. Similar to the AHE loops, magnetic hysteresis loops shrink with increasing temperature and then disappear completely when the temperature is increased to ~80 K. The minor discrepancy in T_c can be attributed to the variations in the different measurement configurations. Nonetheless, it is rather interesting that as the coupling effect assisted by graphene is removed, the system only consisting of freestanding Ni nano-islands exhibits superparamagnetism with a block temperature (T_B) at 20 K (fig. S7), which is much lower than the Curie temperature of the Ni nano-islands/graphene system. The comparison suggests that the existence of 2DEG provided by the single-crystalline graphene enables effective coupling of the discrete superparamagnetic Ni nano-islands leading to stable global 2D ferromagnetism.

The evidence of ferromagnetism in graphene

XMCD measurements are carried out by the total electron yield (TEY) method to confirm the exchange coupling effect between graphene and Ni nano-islands, as shown in Fig. 3. The Ni $L_{2,3}$ absorption spectrum in Fig. 3A shows two strong peaks at 855 and 872 eV, which correspond to the L_3 and L_2 edges, respectively. The spin (M_S) and orbital (M_L) magnetic moments are evaluated by the following sum rules (*29*)

$$M_S = \frac{2\,n_h\,\mu_B}{P_{circ}} \frac{\int_{L_3}(\mu^+ - \mu^-)\,dE - 2\int_{L_2}(\mu^+ - \mu^-)\,dE}{\int_{L_{2,3}}(\mu^+ + \mu^-)\,dE} \quad \text{and} \quad (2)$$

$$M_L = \frac{4}{3}\frac{n_h\,\mu_B}{P_{circ}} \frac{\int_{L_{2,3}}(\mu^+ - \mu^-)\,dE}{\int_{L_{2,3}}(\mu^+ + \mu^-)\,dE} \quad (3)$$

where n_h is the number of 3d holes of Ni and calculated as 1.50 according to DFT calculations as shown below. P_{circ} indicates that the degree of circular polarization of the incoming photons is about 95%. Therefore, $M_S = 0.04\ \mu_B$ and $M_L = 0.10\ \mu_B$. The large ratio of $\frac{M_L}{M_S} = 2.5$ shows that the unquenched orbital moment is related to the nanoscale characteristics of the Ni nano-islands (*30*). Figure 3B exhibits the x-ray absorption spectroscopy (XAS) result of the C-K absorption edge. The regions of 283 to 289 eV and 289 to 300 eV in XAS spectra are attributed to C 1s → π* and 1s → σ* transitions, respectively. Different from the standard XAS spectrum of graphene (*31*, *32*), the delicate and broadened features shown by the C-K edge originate from C 2p–Ni 3d hybridization and charge transfer (*33*). Because of the surface sensitivity of the TEY method, the C XAS signal can only come from the uncovered graphene between adjacent Ni nano-islands, and the corresponding XMCD spectrum reveals induced ferromagnetism in graphene between Ni nano-islands

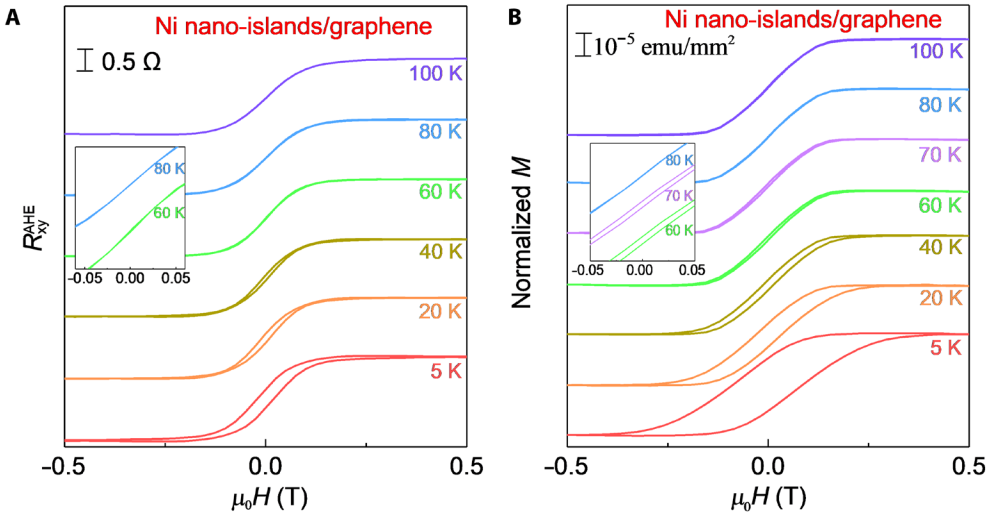

Fig. 2. Magnetization of Ni-nano-islands/graphene. (**A** and **B**) Hall resistance R_{xy}^{AHE} curves and magnetic hysteresis loops in the temperature range from 5 to 100 K under perpendicular magnetic fields. All the curves are shifted vertically for clarity. Inset: Enlarged curves at the corresponding temperature from −0.05 to 0.05 T. emu, electromagnetic unit.

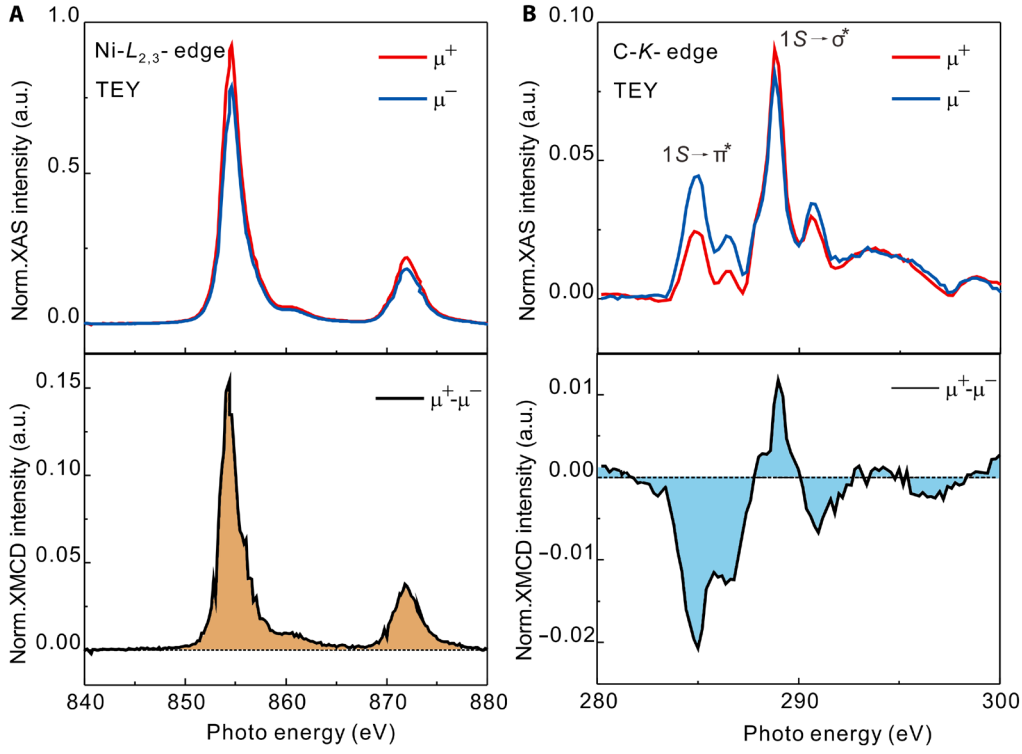

Fig. 3. XMCD spectra of the Ni nano-islands/graphene system. (**A**) XAS spectra of Ni-$L_{2,3}$ and (**B**) C-*K* absorption edges measured with right– and left–circularly polarized light (red and blue) at 15 K after subtracting the smooth background. The corresponding XMCD spectra are shown in the bottom panels. a.u., arbitrary units.

unambiguously. To determine the orbital magnetic moment (M_L) of graphene quantitatively, the following sum rule is used (*34*, *35*)

$$M_L = \frac{2}{3}\frac{n_h \mu_B}{P_{\text{circ}}}\frac{\int(\mu^+ - \mu^-)\,dE}{\int(\mu^+ + \mu^-)\,dE} \quad (4)$$

The number of holes in the C 2*p* orbital is $n_h = 3.06$ according to DFT calculations and so $M_L = -0.21\ \mu_B$. The estimated magnetic moment of the Ni nano-islands/graphene system is larger than that of the graphene/Ni (111) system (*33*) by a factor of more than 2 but similar to that of the graphene/Fe/Ni (111) system (*36*). The opposite sign of the orbital magnetic moments of C and Ni shows possible antiferromagnetic coupling between graphene and Ni nano-islands. Since XMCD is unable to provide the spin moment information of C, antiferromagnetic coupling between the spin moments of graphene and Ni is verified by DFT calculations as shown below. The XMCD results provide clear evidence that the graphene plays an important role in mediating ferromagnetic coupling between discrete Ni nano-islands.

Our systematic investigation of the magnetic properties of the Ni nano-islands/graphene system leads to the following conclusions. First of all, the nanoscale freestanding Ni nano-islands are superparamagnetic with a block temperature of 20 K. Second, pure graphene is nonferromagnetic. Third, the Ni nano-islands/graphene hybrid shows ferromagnetic characteristics up to 80 K, and fourth, coupling between the Ni nano-islands and graphene is antiferromagnetic. The ferromagnetic mechanism of Ni nano-islands/graphene is further clarified. After deposition of Ni nano-islands on single-crystal graphene, single-domain ferromagnetic Ni nano-islands polarize the adjacent graphene and couple with neighboring nano-islands via spin-polarized graphene. At a high temperature (>80 K), ferromagnetic coupling between Ni nano-islands is destroyed by thermal fluctuation and so the hybrid is paramagnetic. When temperature is lower than 80 K, coupling between neighboring Ni nano-islands mediated by graphene suppresses the thermal fluctuation and the hybrid becomes ferromagnetic. Hence, graphene plays a key role in mediating exchange coupling among the discrete Ni nano-islands. As the Fermi level of graphene is closely related to the carrier density, ferromagnetism can be expected to be tunable by varying the gate voltage.

The gate-tunable AHE in the Ni nano-islands/graphene system

Because of the gate-tunable carrier density and polarity of graphene, AHE of the Ni nano-islands/graphene hybrid can be tuned by the gate voltage, as shown in Fig. 4. Figure 4A shows the R_{xy} curves at gate voltages ranging from −60 to 60 V in a step of 10 V at $T = 5$ K. All the curves show a clear hysteresis loop but with a different slope and sign of the NHE background, indicating that the carriers gradually change from holes to electrons as the gate voltage is changed from −60 to 60 V. Figure 4B shows the corresponding R_{xy}^{AHE} loops after subtracting the NHE component. All the R_{xy}^{AHE} loops have a similar shape but different values of saturation magnetoresistance R_{sat}^{AHE} (R_{xy}^{AHE} value at 0.5 T). The extracted R_{sat}^{AHE} is plotted in Fig. 4C as a function of gate bias, and it shows an inverted "V" shape with the maximum at −10 V. According to Eq. 1, the gate-dependent R_{xy}^{AHE} may be attributed to the tunable carrier density or ferromagnetism. However, T_c is independent of the gate voltage (fig. S8), thereby

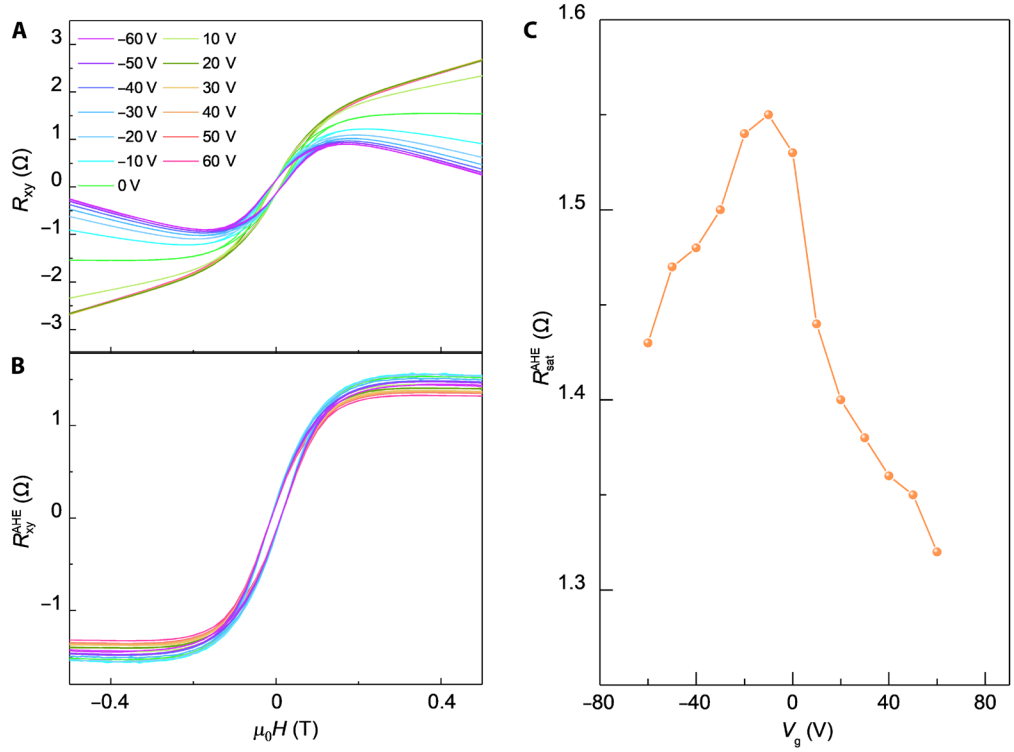

Fig. 4. Gate-tunable AHE in the Ni nano-islands/graphene hybrid. (**A**) Hall resistance R_{xy} and (**B**) R_{xy}^{AHE} as a function of the magnetic field at different gate voltages V_g from −60 to 60 V for steps of 10 V at $T = 5$ K. (**C**) Saturation magnetoresistance R_{sat}^{AHE} as a function of gate voltages from −60 to 60 V at $T = 5$ K.

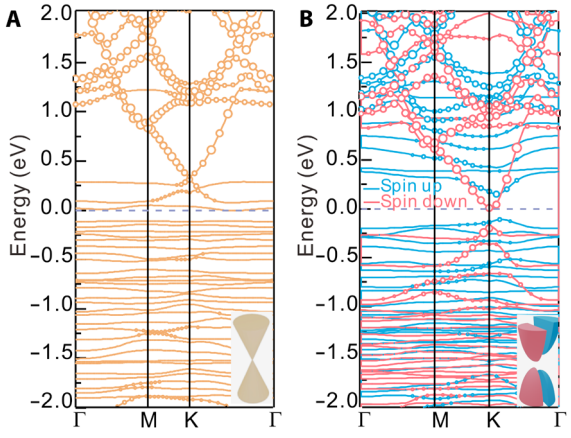

Fig. 5. First-principles calculations. (**A**) Band structure for the LDA calculations of the 8-Ni cluster on graphene (inset: schematic of the band structure). (**B**) Band structure for the LSDA + U calculations of the 8-Ni cluster on graphene. The red and blue lines show the spin down and up bands, respectively. The circles indicate the contribution from graphene, and the diameter is proportional to the weight of the graphene states. The inset shows the schematic of the spin model.

excluding the change of ferromagnetic coupling between the Ni nano-islands and graphene. In addition, the inverted "V" shape of R_{xy}^{AHE} is reminiscent of the carrier density of graphene around Dirac point, as shown by the plot of sheet resistance R_s versus gate bias shown in fig. S9, implying that R_{sat}^{AHE} has a close relationship with the carrier density and Fermi level of graphene. It should be noted that the gate-tunable AHE behavior is also found in graphene proximity coupled to an array of Fe_3O_4 magnetic nanoparticles (MNPs) (*17*). Compared to the MNPs/graphene system, the amount of tunability in our study is relatively small, but the trends are quite similar.

The DFT calculations reveal the origin of ferromagnetism of graphene in the Ni nano-islands/graphene system

To further explore the origin of ferromagnetism, first-principles calculations are carried out on the Ni nano-islands/graphene hybrid. A Ni cluster with eight atoms on graphene is adopted to simulate the Ni nano-islands on the graphene sheet (fig. S10). After the structure is fully relaxed, the electronic structure of the 8-Ni cluster on graphene is derived. According to the experimental results, the system has paramagnetic states at high temperature and ferromagnetism at low temperature. Thus, the nonmagnetic local density approximation (LDA) is implemented to study the high-temperature paramagnetic state (Fig. 5A). The spin-polarized local spin density approximation + Hubbard (LSDA + U) is used to calculate the low-temperature ferromagnetic state (Fig. 5B). It is found that the Dirac point of graphene at the K point is still degenerate, indicating a nonmagnetic metallic state at high temperature as shown in Fig. 5A. However, the spin-polarized calculations in Fig. 5B show that the bands of graphene are split at a low temperature due to C 2*p* and Ni 3*d* hybridization (fig. S11). Spin down shifts closer to the Fermi level and spin up moves to higher energy, indicating that graphene is spin-polarized, leading to the creation of ferromagnetism. Besides, the Dirac point at the K point of monolayer graphene has a gap. The spin down component has a gap of ~0.17 eV and the spin up one has a gap of ~0.25 eV. The system undergoes the metal-insulator transition from the high-temperature nonferromagnetism

metallic state to the low-temperature ferromagnetic state. The transition from the metal state to the insulator state is also suggested by the fact that the total resistance of Ni nano-islands/graphene system decreases as the temperature decreases in the high-temperature regime (300 to 50 K), while it increases as the temperature decreases in the low-temperature regime (<50 K), as depicted in Fig. 1F. The spin magnetic moments of C and Ni in different positions are presented in tables S1 and S2, respectively. The opposite sign of the spin magnetic moments of C and Ni indicates antiferromagnetic coupling between graphene and Ni nano-islands in agreement with the XMCD measurements, and the antiferromagnetic coupling is believed to be ascribed for the charge transfer from Ni atoms of Ni nano-islands to C atoms of graphene (fig. S12). The same calculations are performed on systems consisting of 7, 9, and 10 Ni atoms on graphene (figs. S13 and S14), which are similar to the system consisting of 8 Ni atoms on graphene, to verify the generality. The results reveal that in the Ni nano-islands/graphene system, graphene is spin-polarized and antiferromagnetic coupling occurs between graphene and Ni nano-islands mediated by spin-polarized graphene.

In summary, a 2D ferromagnetic system consisting of superparamagnetic Ni nano-islands and single-crystal graphene is fabricated. XMCD measurements and DFT calculations clarify that graphene is spin-polarized due to the influence of the Ni nano-islands. Global ferromagnetism is established as a result of antiferromagnetic exchange coupling between ferromagnetic graphene and superparamagnetic Ni nano-islands mediated by graphene. The results reveal an ideal platform to obtain high-quality 2D ferromagnetism that can be implemented in 2D spintronic devices.

MATERIALS AND METHODS

Graphene synthesis and transfer

The single-crystalline graphene film was synthesized on Ge (110) and transferred to a 300-nm SiO_2/Si substrate by the PMMA-assisted wet transfer method. A thin layer of PMMA (MicroChem 950 PMMA C, 3% in chlorobenzene) was spin-coated on the graphene/Ge substrate to protect the graphene film. Afterward, the PMMA/graphene/Ge substrate was floated on a mixture of H_2O_2:HF:H_2O (1:1:10) to etch the Ge substrate. The remaining PMMA/graphene was transferred to deionized water for cleaning and then transferred to the 300-nm SiO_2/Si substrate. After drying the PMMA/graphene film, acetone was used to dissolve the PMMA. Last, the graphene/SiO_2/Si was annealed under a mixture flowing argon and hydrogen (5:1) for 3 hours at 100°C to remove the residual PMMA.

Device fabrication and measurements

The Hall bar device was fabricated as schematically illustrated in fig. S2. The Hall electrodes were patterned by standard photolithography and Au/Ti (100/10 nm) was deposited by electron beam evaporation and lift-off. The graphene channels were patterned by another photolithographic step with the aid of an inductively coupled plasma. Last, the 8-nm-thick Ni was deposited on graphene by electron beam evaporation using a stencil mask. The R-T curves and R_{xy}-$\mu_0 H$ curves were measured on the PPMS (Quantum Design), and magnetization was assessed on the MPMS-3 (Quantum Design). The XMCD measurements were performed using the BL08U1A beamline at the Shanghai Synchrotron Radiation Facility by the TEY method.

First-principles calculations

The calculations were performed with the Vienna ab initio simulation package (*37*) using the spin-polarized LDA for electron-electron interactions and projector augmented wave method for electron-ion interactions (*38*). A Coulomb repulsion U of 2.5 eV was considered. A kinetic energy cutoff of 400 eV was adopted to expand the electronic wave functions and the Brillouin zone integration was done on a 6 by 6 by 1 k-point mesh. The structure included a single-graphene layer with a 4 by 4 unit cell to minimize the interactions between the clusters and n-Ni cluster adsorbed on graphene. The supercell dimension perpendicular to the graphene sheet was set to be 18 Å to avoid the interactions between the n-Ni/graphene structure and periodic images in the z direction. Van der Waals interactions were included by the dispersion-corrected DFT-D3 method of Grimme et al. (*38*). All the geometric structures were fully relaxed by the conjugate gradient algorithm until the force on each atom was smaller than 0.01 eV $Å^{-1}$.

SUPPLEMENTARY MATERIALS

Supplementary material for this article is available at http://advances.sciencemag.org/cgi/content/full/7/30/eabg7054/DC1

REFERENCES AND NOTES

1. S. A. Wolf, D. D. Awschalom, R. A. Buhrman, J. M. Daughton, S. von Monlnar, M. L. Roukes, A. Y. Chtchelkanova, D. M. Treger, Spintronics: A spin-based electronics vision for the future. *Science* **294**, 1488–1495 (2001).
2. I. Zutic, J. Fabian, S. Das Sarma, Spintronics: Fundamentals and applications. *Rev. Mod. Phys.* **76**, 323–410 (2004).
3. C. Felser, G. H. Fecher, B. Balke, Spintronics: A challenge for materials science and solid-state chemistry. *Angew. Chem. Int. Ed.* **46**, 668–699 (2007).
4. D. D. Awschalom, M. E. Flatte, Challenges for semiconductor spintronics. *Nat. Phys.* **3**, 153–159 (2007).
5. X. Li, X. Wu, Two-dimensional monolayer designs for spintronics applications. *Wiley Interdiscip. Rev. Comput. Mol. Sci.* **6**, 441–455 (2016).
6. X. Wang, S. Parkin, Q. K. Xue, Preface to special topic: 2D spintronics. *APL. Mater.* **4**, 032201 (2016).
7. W. Han, Perspectives for spintronics in 2D materials. *APL. Mater.* **4**, 032401 (2016).
8. Y. Liu, C. Zeng, J. Zhong, J. Ding, Z. M. Wang, Z. Liu, Spintronics in two-dimensional materials. *Nanomicro Lett.* **12**, 93 (2020).
9. X. Lin, W. Yang, K. L. Wang, W. Zhao, Two-dimensional spintronics for low-power electronics. *Nat. Electron.* **2**, 274–283 (2019).
10. D. L. Cortie, G. L. Causer, K. C. Rule, H. Fritzsche, W. Kreuzpaonter, F. Klose, Two-dimensional magnets: Forgotten history and recent progress towards spintronic applications. *Adv. Funct. Mater.* **30**, 1901414 (2020).
11. A. A. Khajetoorians, J. Wiebe, B. Chilian, S. Lounis, S. Blugel, R. Wiesendanger, Atom-by-atom engineering and magnetometry of tailored nanomagnets. *Nat. Phys.* **8**, 497–503 (2012).
12. J. Ren, H. Guo, J. Pan, Y.-F. Zhang, Y. Yang, X. Wu, S. Du, M. Ouyang, H.-J. Gao, Interatomic spin coupling in manganese clusters registered on graphene. *Phys. Rev. Lett.* **119**, 176806 (2017).
13. P. Blonski, J. Hafner, Geometric and magnetic properties of Pt clusters supported on graphene: Relativistic density-functional calculations. *J. Chem. Phys.* **134**, 154705 (2011).
14. S. Sahoo, S. N. Khanna, P. Entel, Controlling the magnetic anisotropy of Ni cluster supported on graphene flakes with topological defects. *Appl. Phys. Lett.* **107**, 043102 (2015).
15. S. Sahoo, M. F. Islam, S. N. Khanna, Using graphene to control magnetic anisotropy and interaction between supported clusters. *New J. Phys.* **17**, 053052 (2015).
16. X. J. Liu, C.-Z. Wang, H.-Q. Lin, K.-M. Ho, Magnetic moment enhancement for Mn_7 cluster on graphene. *J. Phys. Chem. C* **118**, 19123–19128 (2014).
17. G. Song, M. Ranjbar, D. R. Daughton, R. A. Kiehl, Nanoparticle-induced anomalous Hall effect in graphene. *Nano Lett.* **19**, 7112–7118 (2019).
18. B. Peng, X. Zhang, D. G. A. L. Aarts, R. P. Dullens, Superparamagnetic nickel colloidal nanocrystal clusters with antibacterial activity and bacteria binding ability. *Nat. Nanotechnol.* **13**, 478–482 (2018).
19. G. Wang, M. Zhang, Y. Zhu, G. Ding, D. Jiang, Q. Guo, S. Liu, X. Xie, P. K. Chu, Z. Di, X. Wang, Direct growth of graphene film on germanium substrate. *Sci. Rep.* **3**, 2465 (2013).

20. M. Huang, M. Biswal, H. J. Park, S. Jin, D. Qu, S. Hong, Z. Zhu, L. Qiu, D. Luo, X. Liu, Z. Yang, Z. Liu, Y. Huang, H. Lim, W. J. Yoo, F. Ding, Y. Wang, Z. Lee, R. S. Ruoff, Highly oriented monolayer graphene grown on a Cu/Ni(111) alloy foil. *ACS Nano* **12**, 6117–6127 (2018).
21. A. K. Geim, K. S. Novoselov, The rise of graphene. *Nat. Mater.* **6**, 183–191 (2007).
22. Z. Zhang, A. Matsubayashi, B. Grisafe, J. U. Lee, J. R. Lloyd, Characterization of magnetic Ni clusters on graphene scaffold after high vacuum annealing. *Mater. Chem. Phys.* **170**, 175–179 (2016).
23. J. Wang, A. M. DaSilva, C. Z. Chang, K. He, J. K. Jain, N. Samarth, X. C. Ma, Q. K. Xue, M. H. W. Chan, Evidence for electron-electron interaction in topological insulator thin films. *Phys. Rev. B* **83**, 245438 (2011).
24. H. Xue, Y. Hong, C. Li, J. Meng, Y. Li, K. Liu, M. Liu, W. Jiang, Z. Zhang, L. He, R. Dou, C. Xiong, J. Nie, Large negative magnetoresistance driven by enhanced weak localization and Kondo effect at the interface of $LaAlO_3$ and Fe-doped $SrTiO_3$. *Phys. Rev. B* **98**, 085305 (2018).
25. X. Li, J. Zhuang, Y. Sun, J. Bai, Z. Zafar, Z. Ni, B. Jin, Z. Shi, Enhancement of weak localization for nitrogen-doped graphene by short range potentials. *Carbon* **82**, 346–352 (2015).
26. Y. Tian, L. Ye, X. Jin, Proper scaling of the anomalous Hall effect. *Phys. Rev. Lett.* **103**, 087206 (2009).
27. Y. Deng, Y. Yu, Y. Song, J. Zhang, N. Z. Wang, Z. Sun, Y. Yi, Y. Z. Wu, S. Wu, J. Zhu, J. Wang, X. H. Chen, Y. Zhang, Gate-tunable room-temperature ferromagnetism in two-dimensional Fe_3GeTe_2. *Nature* **563**, 94–99 (2018).
28. H. Ohno, D. Chiba, F. Matsukura, T. Omiya, E. Abe, T. Dietl, Y. Ohno, K. Ohtani, Electric-field control of ferromagnetism. *Nature* **408**, 944–946 (2000).
29. H. Vita, S. Bottcher, P. Leicht, K. Horn, A. B. Shick, F. Maca, Electronic structure and magnetic properties of cobalt intercalated in graphene on Ir(111). *Phys. Rev. B* **90**, 165432 (2014).
30. H. Shiozawa, A. Briones-Leon, O. Domanov, G. Zechner, Y. Sato, K. Suenaga, T. Saito, M. Eisterer, E. Weschke, W. Lang, H. Peterlik, T. Pichler, Nickel clusters embedded in carbon nanotubes as high performance magnets. *Sci. Rep.* **5**, 15033 (2015).
31. B. J. Schultz, C. J. Patridge, V. Lee, C. Jaye, P. S. Lysaght, C. Smith, J. Barnett, D. A. Fischer, D. Prendergast, S. Banerjee, Imaging local electronic corrugations and doped regions in graphene. *Nat. Commun.* **2**, 372 (2011).
32. G. Wang, M. Zhang, D. Chen, Q. Guo, X. Feng, T. C. Niu, X. Liu, A. Li, J. Lai, D. Sun, Z. Liao, Y. Wang, P. K. Chu, G. Ding, X. Xie, Z. Di, X. Wang, Seamless lateral graphene p-n junctions formed by selective in situ doping for high-performance photodetectors. *Nat. Commun.* **9**, 5168 (2018).
33. M. Weser, Y. Rehder, K. Horn, M. Sicot, M. Fonin, A. B. Preobrajenski, E. N. Voloshina, E. Goering, Y. S. Dedkov, Induced magnetism of carbon atoms at the graphene/Ni(111) interface. *Appl. Phys. Lett.* **96**, 012504 (2010).
34. B. T. Thole, P. Carra, F. Sette, G. van der laan, X-ray circular-dichroism as a probe of orbital magnetization. *Phys. Rev. Lett.* **68**, 1943–1946 (1992).
35. P. Carra, B. T. Thole, M. Altarelli, X. Wang, X-ray circular dichroism and local magnetic fields. *Phys. Rev. Lett.* **70**, 694–697 (1993).
36. M. Weser, E. N. Voloshina, K. Horn, Y. S. Dedkov, Electronic structure and magnetic properties of the graphene/Fe/Ni(111) intercalation-like system. *Phys. Chem. Chem. Phys.* **13**, 7534–7539 (2011).
37. M. Cococcioni, S. de Gironcoli, Linear response approach to the calculation of the effective interaction parameters in the LDA + U method. *Phys. Rev. B* **71**, 035105 (2005).
38. S. Grimme, J. Antony, S. Ehrlich, H. Krieg, A consistent and accurate ab initio parametrization of density functional dispersion correction (DFT-D) for the 94 elements H-Pu. *J. Chem. Phys.* **132**, 154104 (2010).

Acknowledgments

Funding: We thank the Key Research Project of Frontier Science, the Chinese Academy of Sciences (QYZDB-SSW-JSC021), the National Science and Technology Major Project (2016ZX02301003), the Science and Technology Innovation Action Plan of Shanghai Science and Technology Committee (20501130700), the National Natural Science Foundation of China (grant nos. 61851401, 61974157, 51925208, U1632266, 11927807, 61905270, and 11804160), the Strategic Priority Research Program (B) of the Chinese Academy of Sciences (XDB30030000), the Natural Science Foundation of Shanghai (no. 19ZR1467100), the Jiangsu Province Science Foundation for Youth (BK20170821), the City University of Hong Kong Strategic Research Grant (SRG) (no. 7005505), and the Science and Technology Commission of Shanghai Municipality (19JC1415500). T.H. acknowledges the support of the National Natural Science Foundation of China (grant no. 11574338). **Author contributions:** Z.D., M.Z., and S.Q. conceived the project. M.G. and X.H. designed and performed the experiments. M.G., X.H., and Z.T. conducted the material growth. E.K. and Y.D. performed the DFT calculations. M.G., X.H., W.L., Y.M., P.K.C., and T.H. performed the data analysis and cowrote the paper. All authors discussed the results and commented on the manuscript. **Competing interests:** The authors declare that they have no competing interests. **Data and materials availability**: All data needed to evaluate the conclusions in the paper are present in the paper and/or the Supplementary Materials. Additional data related to this paper may be requested from the authors.

Submitted 23 January 2021
Accepted 7 June 2021
Published 23 July 2021
10.1126/sciadv.abg7054

Citation: M. Gao, X. Han, W. Liu, Z. Tian, Y. Mei, M. Zhang, P. K. Chu, E. Kan, T. Hu, Y. Du, S. Qiao, Z. Di, Graphene-mediated ferromagnetic coupling in the nickel nano-islands/graphene hybrid. *Sci. Adv.* **7**, eabg7054 (2021).